Monte Carlo simulations of Rb$_2$MnF$_4$: A classical Heisenberg antiferromagnet in two dimensions with dipolar interaction

Chenggang Zhou,[1] D. P. Landau,[2] and T. C. Schulthess[1]

[1]*Center for Nanophase Materials Sciences, Oak Ridge National Laboratory, P.O. Box 2008, Oak Ridge, Tennessee 37831-6493, USA*
[2]*Center for Simulational Physics, University of Georgia, Athens, Georgia 30602, USA*

We study the phase diagram of a quasi-two-dimensional magnetic system Rb$_2$MnF$_4$ with Monte Carlo simulations of a classical Heisenberg spin Hamiltonian which includes the dipolar interactions between Mn^{2+} spins. Our simulations reveal an Ising-like antiferromagnetic phase at low magnetic fields and an *XY* phase at high magnetic fields. The boundary between Ising and *XY* phases is analyzed with a recently proposed finite-size scaling technique and found to be consistent with a bicritical point at $T=0$. We discuss the computational techniques used to handle the weak dipolar interaction and the difference between our phase diagram and the experimental results.

I. INTRODUCTION

The phase diagram of anisotropic Heisenberg antiferromagnets has been studied with renormalization group (RG) methods[1–5] and Monte Carlo simulations.[6–9] In three dimensions, RG calculations for $4-\epsilon$ dimensions and Monte Carlo simulations have found an Ising-like antiferromagnetic (AF) phase at low magnetic fields and an *XY* phase at high fields, separated by a first order spin-flop transition line. The spin-flop transition line terminates at a bicritical point (BCP), where it meets the phase boundary between the *XY* phase and the paramagnetic (PM) phase, and the AF-PM phase boundary. In two dimensions, due to the Mermin-Wagner theorem,[10] a BCP with O(3) symmetry has to be at zero temperature, which was confirmed by RG calculations in $2+\epsilon$ dimensions for the anisotropic nonlinear σ model.[3,5] The *XY*-PM phase boundary and AF-PM phase boundary are exponentially close to each other, while the PM phase sandwiched in between narrows as $\exp(-4\pi/T)$. On the other hand, the continuum field theory of this model contains an infinite number of relevant perturbations beyond the anisotropic nonlinear σ model. Thus, it is also valid to argue that the multicritical point may not be O(3) symmetric and occurs at a finite temperature.[11] One would look for numerical evidence that distinguishes different scenarios. However, Monte Carlo simulations have been unable to trace the phase boundaries of the *XY* and AF phases to sufficiently low temperatures due to the exponentially large correlation length. Recently, a novel finite-size scaling analysis was used to interpret the data from Monte Carlo simulations.[9] It was found that the apparent spin-flop transition line was actually consistent with a zero-temperature BCP. An additional continuous degeneracy in the ground state at the spin-flop field has also been recently discovered.[12] The ground state actually bears some similarities to a tetracritical phase; thus, it was argued that the "hidden bicritical point" might be relabeled as the "hidden tetracritical point."

In real materials, an ideal two-dimensional Heisenberg spin system has not been found, since in a three-dimensional system, the interactions between spins can never be completely restricted to two dimensions. Nevertheless, Rb$_2$MnF$_4$ is a very good quasi-two-dimensional Heisenberg antiferromagnet. In this layered compound, Mn^{2+} ions with spin 5/2 reside on (001) planes, as shown in Fig. 1. Adjacent planes are widely separated by Rb$^+$ ions, so that the exchange interactions between magnetic ions in different planes are negligible. The antiferromagnetic order parameter has been accurately measured with neutron scattering experiments[13] and analyzed with spin-wave theory.[14] The theoretical model with only nearest neighbor exchanges and a staggered magnetic field accounts for the experimental data very well. In the right hand portion of Fig. 1, we show a schematic phase diagram that summarizes the prevailing theoretical alternatives and experimental data for Rb$_2$MnF$_4$. On the other hand, the large magnetic moment of Mn^{2+} ions makes it possible to model the spins with classical vectors. Therefore, it is an excellent system to test theoretical predictions for two-dimensional Heisenberg spin systems, given that the effective anisotropy due to the dipolar interaction is accounted for.[15] Obviously, the dipolar interaction plays an important
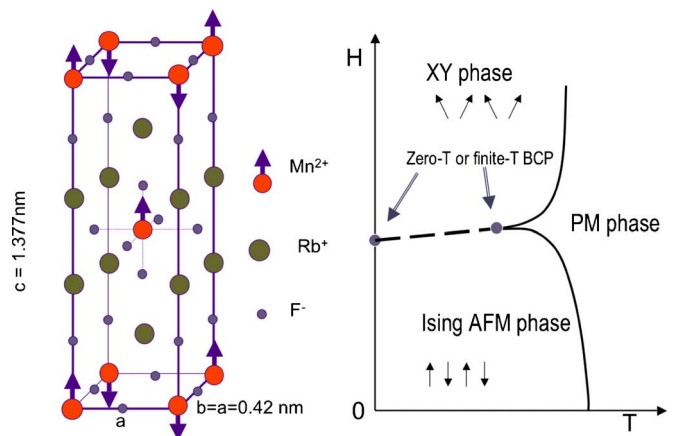

FIG. 1. (Color online) The unit cell of Rb$_2$MnF$_4$ and the schematic phase diagram. If the BCP is at $T=0$, the dashed line actually represents two very close second-order phase boundaries. If the BCP is at a finite temperature, the dashed line represents a single first-order phase transition. The theoretical *XY* phase is found to have transverse AF order in neutron scattering experiments.

role in this system, as it provides the effective anisotropy that stabilizes the low-field AF phase and could mediate a dimensional crossover from two dimensions to three dimensions in the real material. With the in-plane isotropic exchange interaction and the dipolar interaction, the Néel temperature at zero field was calculated by Monte Carlo simulations to be 39.7 ± 0.1 K,[16] slightly higher than the experimental value 38.5 ± 1.0 K.[14,17] Following the previous research,[16] we performed extensive Monte Carlo simulations in both zero and nonzero magnetic fields to construct the full phase diagram and compare it with the experiments.[18] We hope to see our model reproduce the "apparent" BCP at approximately $T = 30$ K, as seen in the experiments. To determine the phase diagram in the thermodynamic limit, we used different finite size scaling analyses for different phase boundaries. In particular, the apparent spin-flop transition has to be examined with the novel finite-size scaling method developed in Ref. 9, and it is actually found to be consistent with a zero-temperature BCP.

The Hamiltonian of our model reads

$$\mathcal{H} = JS(S+1) \sum_{\langle i,j \rangle} \mathbf{S}_i \cdot \mathbf{S}_j - \frac{US^2}{2} \sum_{i \neq j, \alpha, \beta} S_i^\alpha \mathcal{D}_{ij}^{\alpha\beta} S_j^\beta - \sum_i Sg\mu_B \mathbf{h} \cdot \mathbf{S}_i, \tag{1}$$

where $S = 5/2$, $\mathbf{S}_i$ are three-dimensional unit vectors, $J = 0.6544$ meV, the dipolar interaction constant[19] $U = 0.214\,727$ meV Å^3, the Landé g factor $g = 2$, the external magnetic field $\mathbf{h}$ is fixed in the z direction, and the summation over $\langle i,j \rangle$ is over all nearest neighbor pairs. The dipolar interaction tensor $\mathcal{D}$ is given by

$$\mathcal{D}_{ij}^{\alpha\beta} = (3r_{ij}^\alpha r_{ij}^\beta - r_{ij}^2 \delta_{\alpha\beta}) r_{ij}^{-5}. \tag{2}$$

The Mn^{2+} ions are located on a body centered tetragonal lattice, with in-plane lattice constant $a = 4.2$ Å and c-axis lattice constant $c = 13.77$ Å. However, it is known that the dipolar interaction between two tetragonal sublattices nearly vanishes due to the geometric arrangement of the moments.[13,20] Therefore, besides a few simulations with two sublattices performed to check the validity of this assumption, we included only one sublattice in most of our simulations, which allowed us to simplify the dipolar summation and to run simulations for larger systems. Because the interlayer interaction is weak, we have included up to four layers of spins in our simulations, with open boundary condition in the z direction. Each layer is a square lattice with lattice constant equal to a and the distance between adjacent layers equal to c.

The Hamiltonian [Eq. (1)] is an approximation of the actual quantum mechanical Hamiltonian, where spin operators have been replaced with classical vector spins $S\mathbf{S}_i$ or $\sqrt{S(S+1)}\mathbf{S}_i$. Here, some ambiguities arise as to whether S or $\sqrt{S(S+1)}$ should be used. For the dipolar term, we assume that the magnetic field generated by a spin is a dipole field of a magnetic moment $gS\mu_B$, and the dipolar interaction energy of a second spin with moment $gS\mu_B$ in this field is clearly proportional to S^2. This approximation guarantees that the total dipolar energy of a ferromagnetic configuration agrees with macroscopic classical magnetostatics of bulk materials. The exchange term is more ambiguous. One can argue that $S(S+1)$ follows from the quantum mechanical origin of the exchange interaction. After all, the appropriate constant should reproduce the correct spin-wave spectrum or the critical temperature within acceptable error bars. There is no guarantee that both of them can be accurately reproduced with the same classical approximation. In general, by adopting the classical approximation to spins, one admits an error possibly of order $1/S$ in some quantities. To justify our choice in Eq. (1), we first found that the critical temperature at zero field of Eq. (1) was quite close to the experimental value, then we turned on the magnetic fields to explore the full phase diagram. It is unlikely that the entire experimental phase diagram would be reproduced exactly including the spin-flop field. However, our Monte Carlo simulations should exhibit the same critical behavior as the real material, given that they are in the same universality class. In particular, we want to test if there is a "real" BCP at a finite temperature due to the long-range nature of the dipolar interaction.

This paper is organized as follows: In Sec. II, we briefly review the simulation techniques used in this research, especially those designed to handle long-range, but very weak, dipolar interaction. In Sec. III, we present the results from simulations performed near each phase boundary. In Sec. IV, we discuss the results and give our conclusions.

II. MONTE CARLO METHODS

A. Dipole summation

Direct evaluation of the dipolar energy in Eq. (1) should be avoided because the computational cost of direct evaluation scales as $O(N^2)$, where N is the number of spins, and the periodic boundary condition needs to be satisfied. In our simulations, we have as many as 8×10^4 spins and need to evaluate the dipolar energy repeatedly. Therefore, a fast algorithm for dipolar interaction is required. We used the Benson and Mills algorithm[21] which employs the fast Fourier transformation of the spins to reduce the computational cost to $O(N \ln N)$. After Fourier transform, the dipolar sum in Eq. (1) can be written as

$$\sum_{n,n',\alpha,\beta,\mathbf{q}} D_{nn'}^{\alpha\beta}(\mathbf{q}) S_n^\alpha(\mathbf{q}) S_{n'}^\beta(-\mathbf{q}), \tag{3}$$

where n and n' label the different layers of the system, $\mathbf{q}$ is the in-plane wave vector, and $D_{nn'}^{\alpha\beta}(\mathbf{q})$ is the Fourier transform of $\mathcal{D}_{ij}^{\alpha\beta}$. This expression is less costly to evaluate than Eq. (2), since the double summation over all the spins is replaced by a single summation over the wave vectors, and $D_{nn'}^{\alpha\beta}(\mathbf{q})$ are constants which can be calculated quickly in the initialization stage of the simulation. Explicit expressions for $D_{nn'}^{\alpha\beta}(\mathbf{q})$ were first derived in Ref. 21, and were reproduced in Ref. 22 with more detail and clarity.

B. Monte Carlo updating scheme and histogram reweighting

In Monte Carlo simulations of magnetic spin systems, cluster algorithms offer the benefit of reduced correlation times. In Ref. 16, the Wolff cluster algorithm[23] was used to generate new spin configurations based on the isotropic exchange term in the Hamiltonian. Although the Wolff algorithm is rejection-free by itself, the new configuration then has to be accepted or rejected with a Metropolis algorithm according to its dipolar and Zeeman energy. The changes in the dipolar energy and Zeeman energy are roughly proportional to the size of the cluster generated by the Wolff algorithm. When these changes are larger than $k_B T$, the number of rejections rapidly increases, leading to a substantially lower efficiency. This problem occurs when the magnetic field is typically several tesla in our simulations. On the other hand, in the paramagnetic phase or one of the ordered phases, the cluster size is small, and the change in dipolar energy is also small. It, thus, becomes redundant to evaluate the dipolar energy after every small change in the spin configuration.

Since there are no rejection free algorithms for the dipolar interaction, and the dipolar energy only contributes a fraction of about 0.1% to the total energy in our simulations, one of our strategies to handle the dipolar interaction is to accumulate a series of single spin flips before evaluating the dipolar energy, then accept or reject this series of flips as a whole with the Metropolis algorithm depending on the change of the dipolar energy. The number of single spin flips for each Metropolis step can be adjusted in the simulation so that the average acceptance ratio is about 0.5, at which the Metropolis algorithm is most efficient. We used the rejection-free heat-bath algorithm[24–26] to perform single spin flips, which handles both the isotropic exchange and Zeeman terms in the Hamiltonian on the same footing.

Although fast Fourier transform significantly reduces the computational cost of dipolar interaction, this part is still the bottleneck of the simulation. Therefore, we want to further reduce the number of dipolar energy evaluations. To this end, we separate a short-range dipolar interaction from the full dipolar interaction. The short-range part can be defined with a cutoff in distance.[27] In our simulations, we have included the up to fifth nearest in-plane neighbor of each spin, and the spins directly above or below it in the adjacent layer of the same sublattice, to form the short-range dipolar interaction. This short-range dipolar interaction can be handled with the heat-bath algorithm on the same footing with the exchange and the Zeeman term. The extra cost of evaluating local fields produced by the additional 22 neighboring spins is insignificant. With this modification in single spin updates, the Metropolis algorithm should be performed with respect to the change in the long-range dipolar interaction, i.e., the difference between the total dipolar energy and the short-range dipolar energy. Since this long-range dipolar energy is typically a small fraction (about 1%) of the total dipolar energy, it is justified to accumulate many single spin flips before refreshing the total dipolar energy.

We have found that the long-range dipolar energy in our simulations is usually a fraction of about 0.001% of the total energy, which is actually comparable to $k_B T$. This allows us to further simplify the above algorithm by removing the Metropolis step in the simulation, while we simply calculate and record the full dipolar energy for each configuration whose energies and magnetizations are stored for histogram reweighting. In the end, we get a Markov chain of configurations from the simulation generated with a modified Hamiltonian,

$$\mathcal{H}' = \mathcal{H}_{\text{exchange}} + \mathcal{H}_{\text{Zeeman}} + \mathcal{H}_{\text{short}}, \quad (4)$$

where the first two terms are the exchange and Zeeman terms in Eq. (1), and the last term is the short-range dipolar interaction. For those configurations selected for computing thermodynamic averages, we calculate and record $\mathcal{H}'$, $\mathcal{H}_{\text{short}}$, their full dipolar energy H_{dipole}, staggered magnetization of each layer

$$\mathbf{M}_l^{\dagger} = \frac{1}{L^2} \sum_{i,j} (-1)^{i+j} \mathbf{S}_{ijl}, \quad (5)$$

where L is the size of each layer and the index l is the layer index, and the average magnetization per spin in the z direction,

$$M_z = \frac{1}{L^2 N_l} \sum_{i,j,l} S_{ijl}^z, \quad (6)$$

where N_l is the number of layers in the system. As we have observed that the interlayer coupling due to the dipolar interaction is very weak, we define the total staggered magnetization $M^{\dagger}$ as

$$M^{\dagger} = \left[N_l^{-1} \sum_l (M_l^{\dagger})^2 \right]^{1/2}. \quad (7)$$

Similarly, the Ising-like AF order parameter is defined as

$$M_z^{\dagger} = \left[N_l^{-1} \sum_l (M_{l,z}^{\dagger})^2 \right]^{1/2}, \quad (8)$$

and the XY order parameter is defined as

$$M_{xy}^{\dagger} = \left[N_l^{-1} \sum_l (M_{l,x}^{\dagger})^2 + N_l^{-1} \sum_l (M_{l,y}^{\dagger})^2 \right]^{1/2}. \quad (9)$$

Note that we have ignored the factor $S g \mu_B$ in the definitions of various magnetizations so that they are normalized to 1 in the antiferromagnetic configuration. Additionally, the fourth-order Binder cumulant for a quantity Q is defined as

$$U_4(Q) = 1 - \frac{\langle Q^4 \rangle}{3 \langle Q^2 \rangle^2}, \quad (10)$$

where $\langle \cdots \rangle$ represents the ensemble average.

The thermodynamic averages with respect to $\mathcal{H}'$ at a temperature and a magnetic field slightly different from the simulation can be obtained with the conventional histogram reweighting technique.[28] To calculate the thermodynamic average with respect to the original Hamiltonian, the weight for each sample should be modified to

$$\exp\left\{-\frac{1}{k_B T'}[\mathcal{H}' - Sg\mu_B M_z(h'-h) + \mathcal{H}_{\text{long}}]\right\}\exp\left(\frac{\mathcal{H}'}{k_B T}\right),$$

$$(11)$$

where $\mathcal{H}_{\text{long}} = \mathcal{H}_{\text{dipole}} - \mathcal{H}_{\text{short}}$, T and h are the temperature and field at which the simulation was performed, while T' and h' are the temperature and field at which the histogram reweighting is done.

The performance of this perturbative reweighting scheme is valid only when $\mathcal{H}_{\text{long}}$ is smaller than or comparable to the thermal energy $k_B T$. For large system sizes, it has the same problem as the conventional histogram reweighting methods, i.e., the overlap of two ensembles defined by $\mathcal{H}$ and $\mathcal{H}'$ decreases exponentially, leading to a very low efficiency. In fact, since both $\mathcal{H}_{\text{dipole}}$ and $\mathcal{H}_{\text{short}}$ are extensive quantities, we expect their difference $\mathcal{H}_{\text{long}}$ to scale as $N_s L^2$. Therefore, it will exceed any given $k_B T$ with a sufficiently large system size. For those large systems, the above simulation scheme has to be modified to increase the overlap between the two ensembles defined by $\mathcal{H}'$ and $\mathcal{H}$. Fortunately, even for our largest size $L=196$, the long-range dipolar energy for a double layer system at about $T=20$ K and $h=6$ T is mostly positive around 4 meV, and is mostly distributed between $k_B T$ and $4k_B T$. Therefore, the perturbative reweighting technique serves to increase the weight on those configurations with lower dipolar energy, which are usually associated with larger Ising order parameter. One might argue that the long-range dipolar interaction could be ignored since it is extremely small. Actually, our simulations show that for the AF-PM and *XY*-PM phase boundaries, the long-range dipolar interaction is indeed negligible, but for the apparent AF-*XY* phase boundary, its effect can be observed. With the perturbative reweighting technique, we gain knowledge of both Hamiltonians, with or without long-range dipolar interaction, simultaneously; hence, we can tell where in the phase diagram the long-range dipolar interaction changes the phase boundaries.

Most of the results presented in the next section were calculated with the perturbative reweighting technique, except part of the results for the apparent spin-flop transition in Sec. III C, where a difference larger than the error bar is observed. For equilibration, we ran two simulations from different initial configurations until their staggered magnetizations converge within statistical fluctuations. Then, each simulation ran for $5 \times 10^6 - 2 \times 10^7$ Monte Carlo steps per spin to accumulate a large amount of data for histogram reweighting. Early results for zero field were compared with simulations with Metropolis rejection-acceptance steps based on the full dipolar interaction; no difference larger than the error bar had been observed.

III. RESULTS

A. Low-field antiferromagnetic transition

The zero-field AF-PM phase transition was studied with Monte Carlo simulations in Ref. 16, where T_c (the Néel temperature) was determined by extrapolating the crossing points of the Binder cumulant. Since we have adopted a
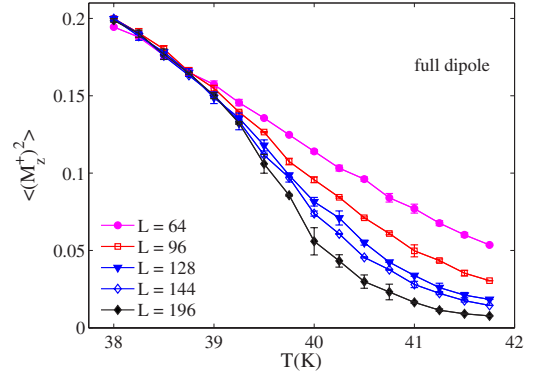

FIG. 2. (Color online) Ising order parameter (staggered magnetization) for double layer systems of different sizes across the zero-field AF-PM phase transition. Data with full dipolar interaction do not differ from those with only short-range dipolar interaction.

slightly different model and also made a number of changes to the Monte Carlo algorithm, we repeated this calculation for testing and calibration purposes. The simulations were performed for double layer systems with $L = 64, 96, 128, 144, 196$. We also calculated the Binder cumulant and performed finite size scaling analysis[29] with Ising critical exponents to fix the Néel temperature. Figure 2 shows the Ising order parameter (total staggered magnetization in the z direction) for different sizes at temperatures close to the Néel temperature. Although the Ising order parameter shows a strong size dependence in the PM phase, the Néel temperature cannot be determined directly from it. The Binder cumulant $U_4(M_z^{\dagger})$ is plotted in Fig. 3. Unlike the results in Ref. 16, where the crossing points of U_4 are above all 40 K, we see in Fig. 3 that all the crossing points are between 39.5 and 40 K. The crossing points of these curves move up toward the universal value of the Ising universality class ($U_4^* \approx 0.618$) as the system size increases. This trend is more clearly revealed by curve fitting with smooth splines, shown
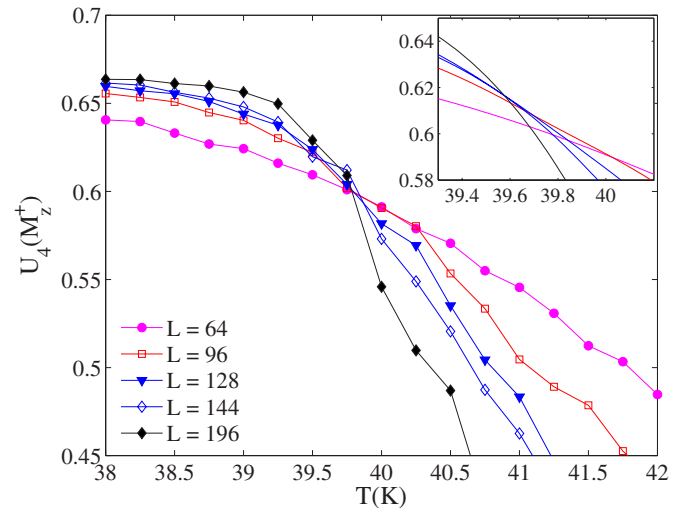

FIG. 3. (Color online) The Binder cumulant for the Ising order parameter across the AF-PM phase transition at zero field. The inset shows a smooth spline fitting of the original data. Crossing points in these curves approach the Ising universal value (≈ 0.618).
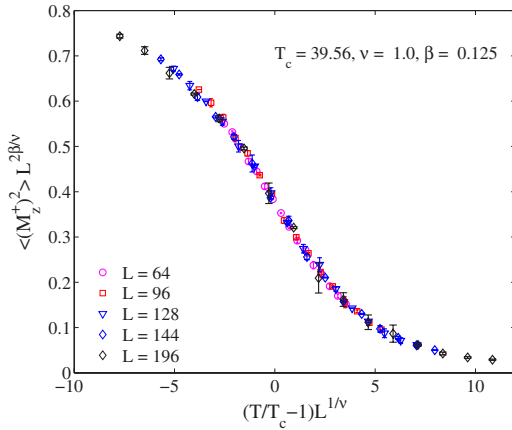
FIG. 4. (Color online) Finite-size scaling analysis of the AF-PM phase transition at zero field. Data points are taken from Fig. 2. All of them fall onto a single curve with Ising critical exponents.
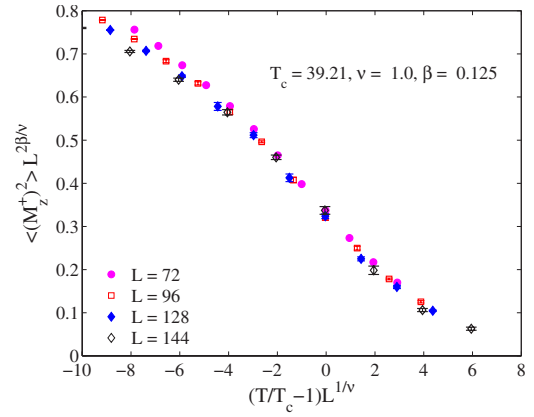

FIG. 5. (Color online) Same scaling plot as Fig. 4, but for simulations performed at $h=3$ T. The critical temperature, at which the best collapsing of data points is achieved, is slightly lower than that of Fig. 4.

in the inset of Fig. 3. Because data points for $\langle (M_z^\dagger)^4 \rangle$ and $\langle (M_z^\dagger)^2 \rangle$ have smaller error bars, we actually did a curve fitting for those two quantities first and plotted the Binder cumulant curve with the fitted functions. T_c can be fixed to be between 39.5 and 39.6 K, where the curves for three larger sizes cross. These observations suggest that the critical behavior of this dipolar two-dimensional Heisenberg antiferromagnet belongs to the Ising universality class. Therefore, we performed a finite size scaling analysis to test this prediction, as well as to fix the Néel temperature more accurately. Figure 4 shows the finite size scaling analysis of the Ising order parameter, where we plot $(T/T_c-1)L^{1/\nu}$ versus $\langle (M_z^\dagger)^2 \rangle L^{2\beta/\nu}$, with Ising critical exponents $\nu=1$ and $\beta=1/8$. Clearly, all the data from different sizes fall nicely on a single curve. The best result is achieved by choosing $T_c=39.56$ K. Obvious deviations from a single curve are seen if T_c changes by 0.1 K; therefore we believe that the error bar for T_c is less than 0.1 K. Although we have obtained a T_c which is only slightly smaller than that obtained in Ref. 16, our data for the Ising order parameter and its Binder cumulant are noticeably different from those in Ref. 16. At the same temperature, data presented here are smaller than those in Ref. 16. This difference is actually expected because of the difference in the strength of the dipolar interaction. The dipolar term is proportional to S^2 here in Eq. (1), but proportional to $S(S+1)$ in the previous work.

We have also performed simulations at $h=3$ and 5 T to study the AF-PM phase transition in a finite magnetic field. The antiferromagnetic phase transition has been observed in both cases, but the order parameter changes more gradually with temperature when the magnetic field is turned on. Finite-size scaling with Ising exponents has been performed. Figure 5 shows the scaling plot of $\langle (M_z)^2 \rangle$ at $h=3$ T, which has a lightly lower T_c. Long-range dipolar interaction only produces negligible changes in these data points. The valid regime for finite-size scaling seems to be narrower than at $h=0$ because some deviations are clearly seen in the low-temperature data points. This could be due to the shape of the phase boundary, which is perpendicular to the temperature axis at $h=0$ by symmetry, but not so at a finite magnetic

field. Because of this, we change both the temperature and the effective anisotropy when the simulation scans temperature at a constant magnetic field.

B. Kosterlitz-Thouless transition

When the magnetic field is above 6 T, the AF-PM phase transition disappears. Instead, the *XY* order parameter [Eq. (9)] becomes large at low temperatures. For a two-dimensional anisotropic Heisenberg antiferromagnet, one expects to see an *XY* phase,[7–9] in which the correlation function decreases algebraically. Since the dipolar interaction breaks the spin rotational symmetry around the *z* axis on a square lattice, one would expect the *XY* phase to be destroyed by its presence. In the case of a ferromagnetic model, it has been shown that above a critical strength, the ferromagnetic dipolar *XY* model exhibits a ferromagnetic phase instead of an *XY* phase.[30] Experimentally, a "transverse" phase with long-range order has been found.[18] However, since the *XY* phase is also very sensitive to small perturbations such as crystal anisotropy and disorder, it is not clear whether the dipolar interaction in Rb$_2$MnF$_4$ alone would prevent it from entering the *XY* phase. To answer this question, we performed simulations in constant magnetic fields $h=6.4$, 6.5, and 7 T at temperatures from 27 to 38 K. Figure 6 shows the *XY* order parameter measured from these simulations for double layer systems with $L=72$, 96, 128, 144, and 196. In all these simulations, the *XY* order parameter increases gradually with lowering temperature in a broad range of temperature, and it is hard to determine the transition temperature from Fig. 6. They also look very different from the results in Ref. 8, where a transition in the *XY* order parameter from zero to a finite value is clearly visible. There are two reasons for this. First, the effective anisotropy induced by dipolar interaction in Rb$_2$MnF$_4$ is very weak. The dipolar energy contributes only about 0.1% to the total energy, while in the anisotropic Heisenberg model studied in Refs. 7–9, the anisotropy is about 10%–20% of the total energy (proportional to the anisotropy constant Δ). Secondly, the magnetic field at which the simulations were performed (6.4–7 T) is still close to the
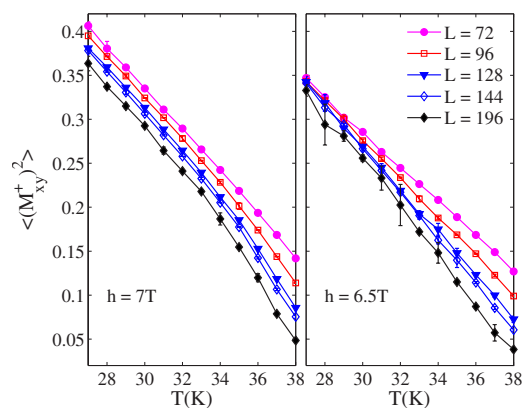
FIG. 6. (Color online) Average XY order parameter across the XY-PM phase boundary for double layer systems with different sizes.

apparent spin-flop transition at about 6.2 T, where the system is effectively an isotropic Heisenberg model. Experimentally, the existence of such an effective Heisenberg model has been tested.[15] Near the apparent spin-flop transition, the system has a large correlation length, which prevents the true XY critical behavior from being revealed in simulations of limited sizes. This also explains why in Fig. 6 $\langle (M_{xy}^{\dagger})^2 \rangle$ increases more rapidly at 7 T with decreasing temperature than it does at 6.5 T.

Nevertheless, we can see in Fig. 6 that the XY order parameter decreases with system size faster at higher temperatures than at lower temperatures. In the PM phase, one expects the size dependence to be exponential, i.e., $\langle (M_{xy}^{\dagger})^2 \rangle \propto \exp(-2L/\xi)$, while in the XY phase, the size dependence is power-law, i.e., $\langle (M_{xy}^{\dagger})^2 \rangle \propto L^{-2\eta}$, where η is a temperature dependent exponent. On the XY-PM phase boundary, the critical value of this exponent is $\eta_c = 1/8$. Therefore, we plot $\langle (M_{xy}^{\dagger})^2 \rangle$ versus L in Fig. 7 with log-log scale, and try to identify the critical temperature for the Kosterlitz-Thouless transition. Below the dashed line in Fig. 7, the order parameter obviously decreases faster than any power law, which would be straight lines in the log-log scale. Above it, the data points are very close to power law, and their slopes decrease
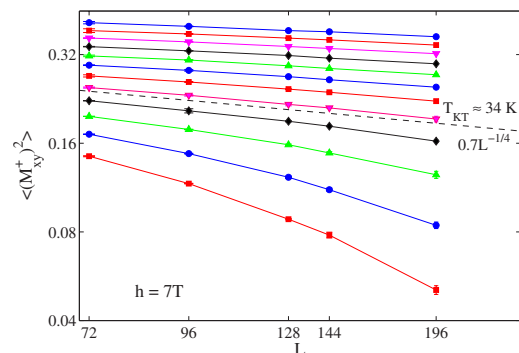

FIG. 7. (Color online) Log-log plot of the size dependence of the XY order parameter. The dashed line is a power law with the critical exponent $2\eta_c = 1/4$, used to identify the critical temperature. For each size, the temperatures of the data points are 27 K, 28 K, ..., 38 K from top to bottom.

with temperature. These features are consistent with an XY-PM phase transition. The critical temperature T_{KT} is roughly 34 K, estimated from Fig. 7. The same analysis has been done for simulations at 6.5 T and the estimated T_{KT} is also near 34 K.

It has been found that if the square anisotropy is strong, the XY model confirms the RG prediction that a second-order phase transition with nonuniversal critical exponents occurs.[31,32] If the anisotropy is weak, two possibilities for the phase diagram have been found by Monte Carlo simulations:[33] (1) a transition from the PM phase directly to the ferromagnetic phase and (2) a narrow XY phase that is sandwiched between the ferromagnetic phase and the PM phase. Both of these cases might appear in our model if we replace the ferromagnetic phase with an antiferromagnetic phase. However, in all simulations performed above $h = 6.4$ T, at the lowest temperature $T = 27$ K, XY order parameter decreases with increasing system size. No evidence for this phase is evident, at least for the range of lattice size that could be considered. Based on this observation, we believe that if a low-temperature in-plane antiferromagnetic phase exists, it does not appear in the range of temperature and magnetic field where our simulations have investigated. Another check to exclude the transition from the PM phase to an Ising-like antiferromagnetic phase is to do the finite-size scaling analysis with Ising exponents for the XY order parameter. We have found that it is impossible to collapse all the data points in Fig. 6 onto a single curve, no matter what critical temperature we use.

We have also performed simulations with a single layer of spins, and the results agreed with those for double layer systems within error bars. The results without perturbative reweighting, i.e., short-range dipolar interaction only, also do not differ noticeably from those with full dipolar interaction presented in Figs. 6 and 7. Therefore, we conclude that our results are consistent with an XY-PM transition. The main effect of the dipolar interaction is to provide an easy axis anisotropy, but the in-plane square anisotropy of the dipolar interaction is not strong enough to destroy the XY phase in the parameter ranges that we have examined.

C. Transition from AF phase to XY phase

Having found an Ising-like AF phase at low magnetic fields and an XY phase at high magnetic fields, we now turn to the boundary between these two phases. Precisely speaking, we want to tell if this boundary exists in the thermodynamic limit, and if it exists, find where it is connected to the XY-PM and AF-PM phase boundaries. So far, we know that our system is best described by a two-dimensional anisotropic Heisenberg antiferromagnet with a very weak long-range interaction of square symmetry. Both the anisotropy and the long-range interaction come from the dipolar interaction. If the long-range component of the dipolar interaction can be completely ignored, the XY-PM phase boundary and the AF-PM phase boundary meet at a zero-temperature BCP, as predicted by the RG theory[4,5] and confirmed by Monte Carlo simulations recently.[9] In this case, there is no real phase boundary between the XY phase and the AF phase.
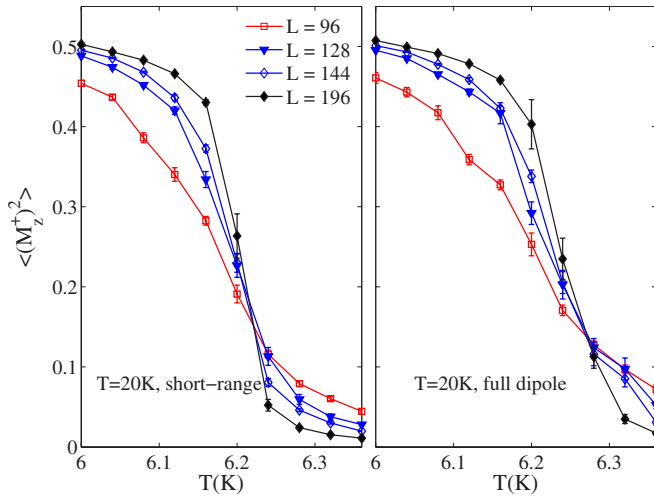
FIG. 8. (Color online) Ising order parameter of double layer systems across the apparent spin-flop transition at $T=20$ K. The data reweighted with full dipolar interaction in the right panel shift toward large magnetic field and have larger error bars.

FIG. 9. (Color online) *XY* order parameter of double layer systems across the apparent spin-flop transition at $T=20$ K. The data reweighted with full dipolar interaction in the right panel shift toward large magnetic field and have larger error bars.

However, if the long-range component of the dipolar interaction is relevant, then the other two possibilities might be favored, i.e., a BCP at a finite temperature or a tetracritical point. In experiment, the neutron scattering data favored a finite temperature BCP, so that the transition from the AF phase to the transverse phase is a first-order phase transition.[18] Whatever brings the transverse phase, which is observed to have long-range order, can also bring the bicritical point to a finite temperature. Because both the transverse phase and the AF phase have discrete symmetries, the BCP is not required to have a continuous (rotational) symmetry. The existence of such a bicritical point at finite temperature does not violate the Mermin-Wagner theorem.

We have performed simulations at constant temperatures $T=5, 10, 20,$ and 30 K and calculated both the Ising order parameter and the *XY* order parameter for magnetic fields between 6 and 6.4 T. We found that a transition apparently occurs at about 6.2 T at all temperatures, and this transition happens over a larger range of magnetic field at higher temperatures than it does at lower temperatures. It must be pointed out that the location of this transition is about 0.9–1.1 T higher than the spin-flop transition in the experimental phase diagram. The transition field also does not show a noticeable temperature dependence, while the experimental spin-flop line has a positive slope. However, our result is in agreement with previous simulations in Ref. 16; therefore, we believe that this difference is a result of the classical approximation we have adopted and also possibly some other weak effects, e.g., crystal field anisotropy, that we have not included in our simulations.

Figure 8 shows the Ising order parameter calculated at $T=20$ K across the transition for different system sizes. The left panel shows the result calculated with only short-range dipolar interaction, and the right panel shows the same data reweighted with full dipolar interaction. The *XY* order parameter which becomes large in higher magnetic fields is shown in Fig. 9. To tell if there is a BCP at a finite temperature, we need to classify the transition we have seen in Figs.
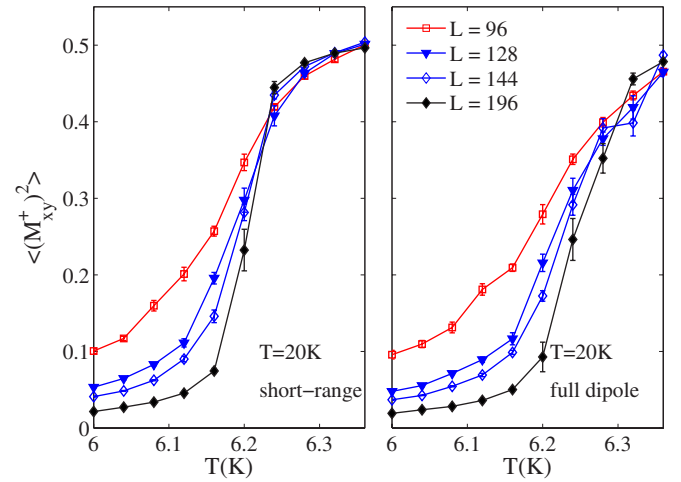
8 and 9 using a finite-size scaling analysis. If it turns out to be a first-order phase transition, a BCP must exist above 20 K. The finite-size scaling for the first-order phase transition was established in Ref. 34. For a BCP at $T=0$, Ref. 9 showed that logarithmic corrections to first-order finite-size scaling would be observed. We plot the Ising order parameter with the scaling ansatz for the zero-temperature BCP[9] in Fig. 10 and with the first-order scaling ansatz in Fig. 11.

In Fig. 10, we have two tunable parameters: the critical field h_c and an effective temperature T^*. The logarithmic corrections, powers of $x=1-T^* \ln L/(2\pi)$, come from the spin renormalization constant calculated by RG for an effective anisotropic nonlinear σ model at T^*, with effective anisotropy vanishing at $h=h_c$. By tuning h_c and T^*, we have collapsed all the data points with short-range dipolar interaction onto a single curve very well. The data with full dipolar interaction also collapse onto a single curve, except for a few
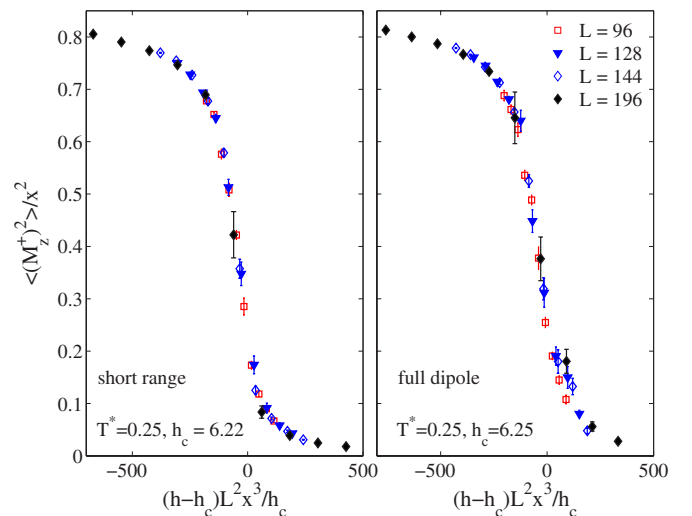

FIG. 10. (Color online) Finite-size scaling plot of the Ising order parameter at $T=20$ K with scaling ansatz for a zero-temperature BCP, where $x=1-T^* \ln L/(2\pi)$.
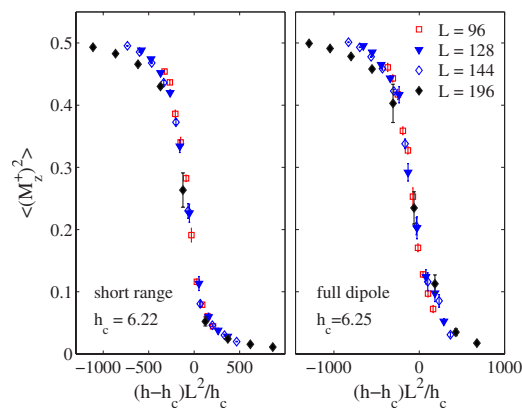
FIG. 11. (Color online) Finite-size scaling plot of Ising order parameter at $T = 20$ K with scaling ansatz for a first-order phase transition, to compare with Fig. 10.

data points with relatively large error bars. Especially on the low-field side of the figure, the quality of collapsing is good. On the other hand, the first-order scaling plot in Fig. 11 shows clear systematic deviation in the low-field data points. This deviation is seen in both the left panel for short-range dipolar interaction and the right panel for full dipolar interaction. The only effect of the long-range part of the dipolar interaction is to shift the critical field h_c up by 0.03 T. Although this effect is small, it is clearly out of the error bars of the finite-size scaling analysis. It is also expected from the comparison of the left and right panels in Figs. 8 and 9, where the transition with the full dipolar interaction clearly shifts to higher magnetic fields.

The same scaling analysis applies to the XY order parameters as well. Figure 12 finite-size XY order parameter at $T = 20$ K calculated with short-range dipolar interaction. Obviously, the scenario of a zero-temperature BCP fits the data better than a first-order phase transition.

At lower temperatures, the same scaling behavior of order parameters has been observed, and the critical field h_c turns out to be nearly identical. Figure 13 shows the finite-size scaling plots for Ising and XY order parameter calculated at $T = 10$ K. Since the transition at 10 K happens within a narrower range of magnetic field, we have included data points
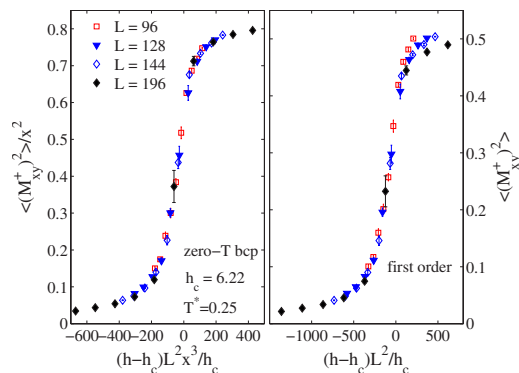

FIG. 12. (Color online) Finite-size scaling of the XY order parameter at $T = 20$ K (comparison of first-order scenario and zero-temperature BCP). The critical field h_c and effective temperature T^* are the same as those in Fig. 10.
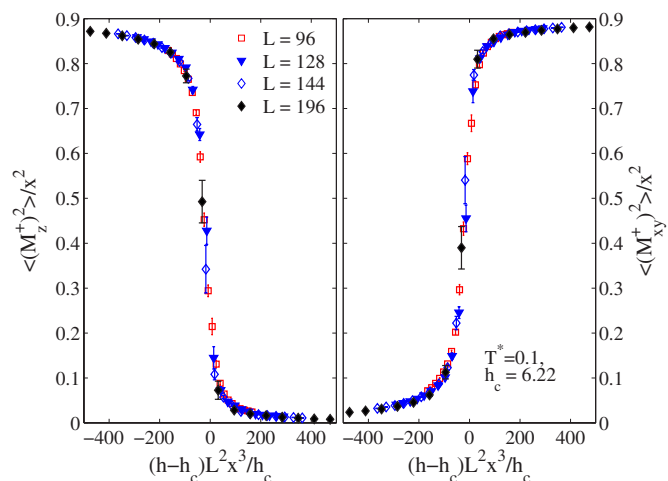

FIG. 13. (Color online) Finite-size scaling of the Ising (left) and XY (right) order parameters calculated at 10 K, corresponding to a zero-temperature BCP. Data shown here are calculated with short-range dipolar interaction for double layer systems, and data with histogram reweighting at different magnetic fields are also shown. $h_c = 6.22$ is the same as that in Fig. 10, while $T^* = 0.1$ is smaller here.

reweighted at fields different from those of the simulation. Data points for $L = 196$ close to the transition which have large error bars are reweighted with different magnetic fields. Nevertheless, most of the data points collapse nicely onto a single curve. For data with short-range dipolar interactions, we have again found $h_c = 6.22$ T, while for data reweighted with full dipolar interaction, the scaling plots look best if we choose $h_c = 6.25$ T.

Therefore, our finite-size scaling so far is more consistent with a zero-temperature BCP than a finite temperature BCP above 20 K. Reference 9 also predicts finite-size scaling relations for the susceptibility and specific heat, and also predicts that the Binder cumulant $U_4(M_z^\dagger)$ is close to, but slightly below, 0.4 at the critical field. We have observed the finite-size scaling behavior of the susceptibility; however, we have not seen behaviors of the Binder cumulant and the specific heat similar to those presented in Ref. 9. For the Binder cumulant, Fig. 14 shows that the curves for three larger sizes cross approximately at $h = 6.203$ T and $U_4 = 0.54$. This value
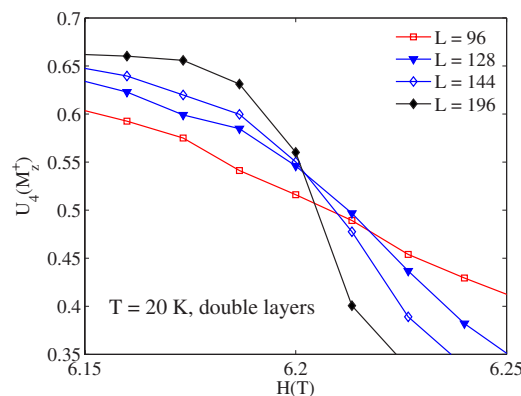

FIG. 14. (Color online) The Binder cumulant of the Ising order parameter; three curves for the larger sizes cross approximately at $h = 6.203$ T and $U_4 = 0.54$.
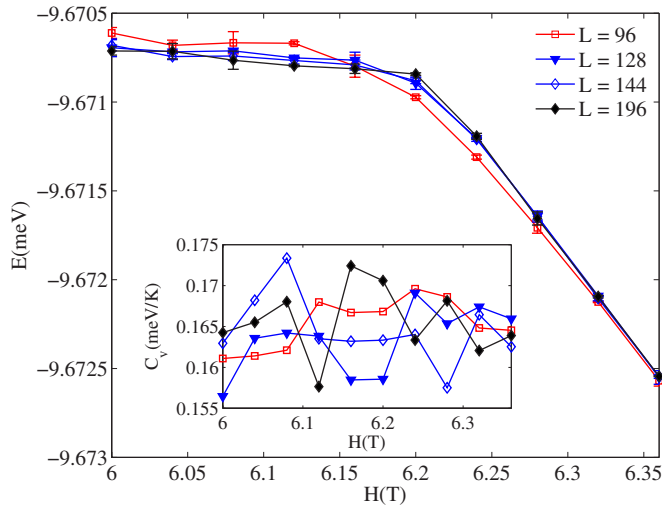
FIG. 15. (Color online) The average energy per spin for a double layer system at $T=20$ K across the apparent spin-flop transition. The inset shows the specific heat per spin, which does not show a peak similar to that of first- or second-order phase transitions.

FIG. 16. Comparison between our phase diagram and the experimental results. The experimental data points from Ref. 18 are plotted in solid squares.

is still very different from the universal value for the Ising universality class. However, this is actually consistent with the theory in Ref. 9, if one notices that here we have *two* nearly independent layers of spins. If there is only one layer, Ref. 9 has shown that at the critical field, the system is effectively a single spin of length ζ with no anisotropy, where ζ is the spin renormalization constant. Its angular distribution is uniform, which implies $\langle (M_z^\dagger)^n \rangle = 1/(n+1)$ and the crossing value of $U_4(M_z^\dagger)$ is approximately 0.4. In our simulations, since we have more than one layer, and they are weakly coupled, we expect that the total staggered magnetization of each layer $\mathbf{M}_l^\dagger$ is uniformly distributed on a sphere of radius ζ. Due to our definition of $M_z^\dagger$ in Eq. (8), the distribution of $M_z^\dagger$ is not a uniform distribution, although $M_{l,z}^\dagger$ of each layer is distributed uniformly. Suppose that the interlayer coupling can be completely ignored, which is a crude approximation. After some simple calculations, we found that the probability distribution of $s=(M_z^\dagger)^2/\zeta^2$ for a double layer system is

$$
P(s) = \begin{cases} \dfrac{\pi}{2}, & 0 < s \leqslant \dfrac{1}{2} \\[2ex] \sin^{-1}\dfrac{1}{\sqrt{2s}} - \sin^{-1}\sqrt{\dfrac{2s-1}{2s}}, & 1 > s > \dfrac{1}{2}. \end{cases}
$$

(12)

Thus, if we ignore both the longitudinal fluctuation of staggered magnetization and the interlayer coupling, the Binder cumulant at the critical field should be $1-\langle s^4 \rangle_P/(3\langle s^2 \rangle_P^2)$. A numerical evaluation of this expression gives 0.5334, which is very close to the crossing point in Fig. 14. Therefore, our simulation is consistent with weakly coupled multiple layers of an anisotropic Heisenberg antiferromagnet.

As for the specific heat, we have not seen a peak at the transition in all our simulations. Figure 15 shows the energy per spin and specific heat per spin calculated for double layer
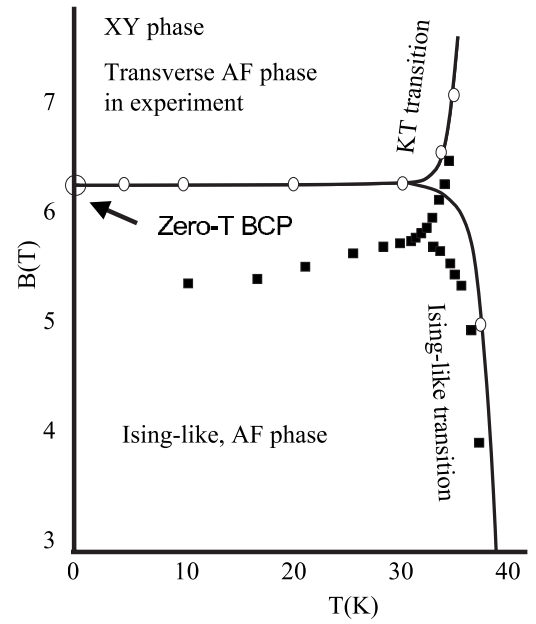
systems at $T=20$ K with short-range dipolar interaction. The energy drops when the magnetic field is larger than the critical field. However, the specific heat shown in the inset does not show any sign of a peak. Although the error bar of the specific heat, as one can estimate from the fluctuation of the data points, is about 10%, a peak which is expected to be similar to those discovered in Ref. 9 is clearly absent. However, this result is actually consistent with the finite-size scaling theory for specific heat in Ref. 9, which shows that the peak in specific heat should be proportional to $(dh_c/dT)^2$. Because the critical field of our model is almost independent of the temperature, i.e., $dh_c/dT \approx 0$, we actually do not expect to see a peak in the specific heat here.

D. Discussions

To summarize our results, we construct a phase diagram in Fig. 16 based on our simulations and compare it to the experimental phase diagram from Ref. 18. Both our *XY*-PM and AF-PM phase boundaries are close to experimental results; the most pronounced difference is the spin-flop line. Rigorously speaking, our spin-flop line is not a single line, but the extensions of *XY*-PM and AF-PM phase boundaries which are exponentially close to each other and meet at a zero-temperature BCP. The experimental *XY*-AF "phase boundary" is empirical. Our spin-flop line is higher in magnetic field than the experimental one and has a nearly vanishing slope, but this difference in spin-flop field is most likely to be a consequence of the classical approximation which omitted quantum fluctuations of the spins. The anisotropic Heisenberg antiferromagnet studied in Ref. 9 offers a simple case to qualitatively analyze this effect. A brief derivation of the spin-flop field of this model is given in the Appendix. If we assume that the length of the classical spins

is $\sqrt{S(S+1)}$, the zero-temperature spin-flop field of this simple model in the classical case is $4J\sqrt{S(S+1)(1-\Delta^2)}$. The spin-flop field of the quantum mechanical Hamiltonian is found to be $4JS\sqrt{1-\Delta^2}$ within the linear spin-wave approximation. More accurate results can be obtained by quantum Monte Carlo simulations; however, the linear spin-wave theory has already considerably reduced the spin-flop field. Since this simple model and the dipolar Heisenberg antiferromagnet studied here have the same critical behavior near the apparent spin-flop transition, one would also expect the quantum effects in the latter model would reduce the spin-flop field by approximately the same amount. Actually, given the classical result $h_c \approx 6.25$ T and assuming that the classical model consists of spins of length $\sqrt{S(S+1)}$, the reduced spin-flop transition would be $h_c/\sqrt{1+1/S} = 5.28$ T, which happens to be in agreement with the experimental value.

Above the spin-flop line, we have observed the *XY* phase, as far as our simulations have covered, while the experiment shows a transverse phase. Therefore, our Hamiltonian certainly misses some weak but important effects in the real material, as the intricate correlation of the *XY* phase and the spin-flop transition is sensitive to many perturbations. Disorder is one of them, which can impose a cutoff in correlation length of the system so that the system would not approach the ideal zero-point BCP from the narrow PM phase. As a result, an apparent finite temperature BCP would be observed and the apparent spin-flop transition below the "BCP" looks like a first-order transition. The disorder can come from both the crystal defects and the slight inhomogeneity in the magnetic field. The experimentally observed finite temperature BCP can also be a result of crossover to three dimensions due to very weak exchange between layers.

The other factor that might have contributed to a phase diagram different from the experimental result is the exchange constant. The spin-wave analysis of Rb_2MnF_4, which provided us the exchange constant *J*, was done for systems in zero magnetic field, and the dipolar interaction had already been simplified to a temperature dependent staggered magnetic field acting on Mn^{2+} spins.[14] Therefore, the exchange integral provided by this theory is an effective quantity that depends on the particular form of the Hamiltonian which has been assumed. As far as we know, similar calculations have not been done in magnetic fields close to the spin-flop transition. Instead, a Hamiltonian with temperature and magnetic field dependent anisotropy has been parametrized to fit the experimental phase diagram.[35] It is not guaranteed that when the full dipolar interaction is used in the Hamiltonian, instead of an effective staggered magnetic field, the exchange integral deduced from a simplified Hamiltonian is still applicable and can be treated as a constant independent of either temperature or magnetic field.

Finally, we show some results that justify two main assumptions, i.e., the inclusion of only a few layers of Mn^{2+} spins and the omission of two sublattices. Figure 17 shows the Ising order parameter across the apparent spin-flop transition for systems with $L=96$ but with different numbers of layers. With short-range dipolar interaction, the result seems to saturate when we have three or more layers. After reweighting with full dipolar interaction, the difference be-
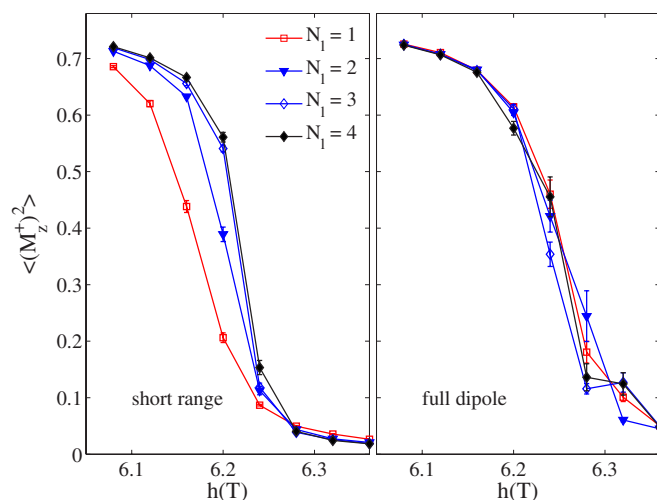

FIG. 17. (Color online) Ising order parameters calculated for systems at $T=10$ K with $L=96$ and different numbers of layers. The thickness dependence is weak. It is more obvious in the left panel, where we only include short-range dipolar interaction, than in the right panel, with full dipole reweighting.

tween data for different numbers of layers becomes even smaller. We estimate the change in h_c due to the change in the number of layers to be of order 0.01 T. Therefore, it is justified to do simulations with only a few layers of spins. The crossover to a three-dimensional system will only occur at very low temperatures. Figure 18 shows a finite-size scaling plot of the apparent spin-flop transition at $T=10$ K calculated with two sublattices. The dipolar interactions between two sublattices were truncated to third nearest neighbors, i.e., a Mn^{2+} spin feels the magnetic field generated by a total of 32 neighboring spins in the Mn^{2+} layer above and below it belonging to the other sublattice. The magnetic field contributed by spins outside this truncation radius should be extremely small based on our experience with the long-range dipolar interaction. Compared with Fig.
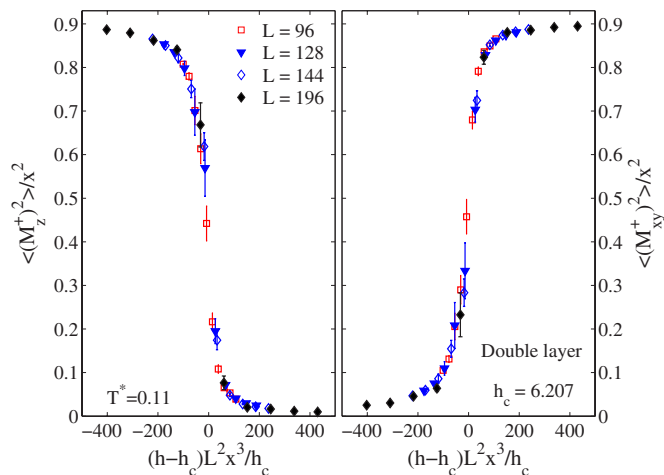

FIG. 18. (Color online) Finite-size scaling plot for simulations at $T=10$ K with intersublattice dipolar interactions. The data in this figure only differ very slightly from those in Fig. 13, in which the intersublattice dipolar interactions were omitted.

13, which was calculated with a single sublattice, the difference in T^* and h_c is negligible. We have enough reason not to expect the interaction between two sublattices to reduce the apparent spin-flop field h_c by more than 0.1 T. The actual additional energy due to the intersublattice dipolar interaction is found to be only comparable to the long-range dipolar energy.

IV. CONCLUSIONS

In conclusion, we have tried to explain the phase diagram of Rb$_2$MnF$_4$ using a classical spin model with dipolar interactions. A large amount of Monte Carlo simulations have been carried out to investigate the phase boundaries. Among different strategies to handle the dipolar interaction in the simulations, we have found our perturbative reweighting technique to be the most suitable for very weak dipolar interactions in Rb$_2$MnF$_4$. The phase diagram inferred from our data captures the main features of the experimental phase diagram and the agreement is good at low magnetic fields. On the apparent spin-flop line, the XY and AF boundaries come so close together that they cannot be distinguished below an "effective" BCP at $T \approx 30$ K. However, our data analyses support a zero-temperature BCP. This conclusion is based on a novel finite-size scaling analysis for two-dimensional anisotropic Heisenberg antiferromagnets.[9] If this multicritical point is located at very low finite temperature, as suggested by Ref. 11, we believe that its temperature must be sufficiently low, which is beyond our numerical accuracy. The ground state degeneracy for the anisotropic Heisenberg antiferromagnets as found in Ref. 12 may also exist in our model with dipolar interactions, which we have not yet verified. If it exists, one might simply rename the bicritical point as a tetracritical point. The zero-temperature BCP is located above the experimental spin-flop line in the phase diagram, which appears to be a line of first-order phase transitions. We believe that this difference from the experimental phase diagram is mainly caused by the classical approximation. Nevertheless, we have confirmed that the dominant effect of the dipolar interaction in Rb$_2$MnF$_4$ is to provide an effective anisotropy, while other effects, such as in-plane square anisotropy and interlayer interaction, are extremely weak. Therefore, we would hope to obtain a more accurate phase diagram if we performed quantum Monte Carlo simulations for a simpler Hamiltonian which includes the effective anisotropy.

APPENDIX: SPIN-FLOP FIELD AT $T=0$ OF ANISOTROPIC HEISENBERG ANTIFERROMAGNET

As an analogy to the dipolar Heisenberg antiferromagnet, we consider the simple anisotropic Heisenberg antiferromagnet with the Hamiltonian

$$\mathcal{H} = J \sum_{\langle i,j \rangle} [\Delta (S_i^x S_j^x + S_i^y S_j^y) + S_i^z S_j^z] - H \sum_i S_i^z, \quad (A1)$$

which is defined on a square lattice. The classical version of this model has been well studied,[7–9] where the spins are treated as unit vectors. The spin-flop field at zero temperature is $H_c = 4J\sqrt{1-\Delta^2}$. If we replace the spins with vectors of length $\sqrt{S(S+1)}$, H_c is then modified to $4J\sqrt{S(S+1)(1-\Delta^2)}$. This is not the only way to make connections to the quantum Hamiltonian. One can also replace J with $JS(S+1)$, while replacing H with HS, which can be justified by arguing that the Zeeman energy of the ferromagnetic configuration takes on the correct macroscopic value. In this case, the spin-flop field is modified to $H_c = 4J(S+1)\sqrt{1-\Delta^2}$. However, in any case, we will show that the classical spin-flop field is larger than the quantum mechanical spin-flop field. By introducing the Holstein-Primakoff (HP) bosons on A and B sublattices, respectively, and keeping the quadratic terms, the Hamiltonian [Eq. (A1)] can be rewritten as

$$\mathcal{H} \approx J \sum_{i \in A} \sum_{\langle j,i \rangle} [\Delta S(a_i^\dagger b_j^\dagger + \text{c.c.}) + (a_i^\dagger a_i - S)(S - b_j^\dagger b_j)]$$
$$- H \sum_{i \in A} a_i^\dagger a + H \sum_{j \in B} b_i^\dagger b, \quad (A2)$$

where a and $a^\dagger$ are HP boson operators on sublattice A and b and $b^\dagger$ on sublattice B, and index i labels sites on sublattice A which are nearest neighbors of the sites on sublattice B labeled with j. After a Fourier transformation, this quadratic Hamiltonian turns out to be

$$\mathcal{H} = -4JS(S+1)N_A - HN_A - \sum_{\mathbf{k}} \mathcal{H}_{\mathbf{k}}, \quad (A3)$$

where N_A is the number of sites on sublattice A, and

$$\mathcal{H}_{\mathbf{k}} = SJ(a_{\mathbf{k}}^\dagger \ b_{-\mathbf{k}}) \begin{pmatrix} 4-h & \Delta\gamma_{\mathbf{k}} \\ \Delta\gamma_{\mathbf{k}} & 4+h \end{pmatrix} \begin{pmatrix} a_{\mathbf{k}} \\ b_{-\mathbf{k}}^\dagger \end{pmatrix}. \quad (A4)$$

For simplicity, we have defined $h = H/SJ$ and $\gamma_{\mathbf{k}} = 2\cos k_x + 2\cos k_y$. The spin-wave spectrum can be obtained with the Bogoliubov transformation:

$$c_{\mathbf{k}} = \cosh \theta_{\mathbf{k}} a_{\mathbf{k}} + \sinh \theta_{\mathbf{k}} b_{-\mathbf{k}}^\dagger, \quad (A5)$$

$$d_{\mathbf{k}} = \sinh \theta_{\mathbf{k}} a_{\mathbf{k}}^\dagger + \cosh \theta_{\mathbf{k}} b_{-\mathbf{k}}. \quad (A6)$$

In order to eliminate the cross terms in the Hamiltonian, one sets $\tanh 2\theta_{\mathbf{k}} = \Delta\gamma_{\mathbf{k}}/4$. Apart from a constant term, the spin-wave part of the Hamiltonian turns out to be

$$\mathcal{H}_{\text{sw}} = \sum_{\mathbf{k}} [\omega_+(\mathbf{k}) d_{\mathbf{k}}^\dagger d_{\mathbf{k}} + \omega_-(\mathbf{k}) c_{\mathbf{k}}^\dagger c_{\mathbf{k}}], \quad (A7)$$

where

$$\omega_\pm(\mathbf{k}) = JS\sqrt{16 - \Delta^2 \gamma_{\mathbf{k}}^2} \pm H. \quad (A8)$$

When H is large enough such that $\omega_-(0)$ becomes negative, the AF ground state becomes unstable since the excitations on spin-wave mode $c_{\mathbf{k}=0}$ lower the ground state energy. This precisely indicates the spin-flop instability. Therefore, the critical magnetic field is given by

$$H_c = 4JS\sqrt{1-\Delta^2}. \qquad\qquad (A9)$$

Although the above spin-wave analysis is only a crude approximation, we see that the quantum effect lowers the spin-flop field by a factor of $S/(S+1)$ or $\sqrt{S/(S+1)}$, depending on which classical approximation one uses. The case with $\Delta = 2/3$ and $S = 1/2$ has been studied with quantum Monte Carlo simulations.[36] Its phase diagram shows that the spin-flop field is at approximately $h/J_{xy} = 1.8$, i.e., $H_c = 1.2J$ in our notation here. The above spin-wave approximation gives $H_c = 1.49J$, and the two classical approximations give $H_c = 4.47J$ and $H_c = 2.58J$, respectively. Clearly, the classical approximations overestimate the spin-flop field. The difference from the real spin-flop field is large as we expect the quantum fluctuation to have a strong effect for $S = 1/2$. For larger spins, such as $S = 5/2$ which is studied in this paper, the classical approximation should work better. However, we still expect it to overestimate the spin-flop field by a noticeable amount.

[1] J. M. Kosterlitz, D. R. Nelson, and M. E. Fisher, Phys. Rev. B **13**, 412 (1976).

[2] D. R. Nelson and J. Rudnick, Phys. Rev. Lett. **35**, 178 (1975).

[3] R. A. Pelcovits and D. R. Nelson, Phys. Lett. **57A**, 23 (1976).

[4] D. R. Nelson, in *Magnetism and Magnetic Materials—1975*, edited by J. J. Becker, G. H. Lander, and J. J. Rhyne, AIP Conf. Proc. No. 29 (AIP, New York, 1976), p. 450.

[5] D. R. Nelson and R. A. Pelcovits, Phys. Rev. B **16**, 2191 (1977).

[6] D. P. Landau and K. Binder, Phys. Rev. B **17**, 2328 (1978).

[7] D. P. Landau and K. Binder, Phys. Rev. B **24**, 1391 (1981).

[8] M. Holtschneider, W. Selke, and R. Leidl, Phys. Rev. B **72**, 064443 (2005).

[9] C. Zhou, D. P. Landau, and T. C. Schulthess, Phys. Rev. B **74**, 064407 (2006).

[10] M. E. Mermin and H. Wagner, Phys. Rev. Lett. **17**, 1133 (1966).

[11] A. Pelissetto and E. Vicari, arXiv:cond-mat/0702273 (unpublished).

[12] M. Holtschneider, S. Wessel, and W. Selke, arXiv:cond-mat/0703135 (unpublished).

[13] R. J. Birgeneau, H. Guggenheim, and G. Shhirane, Phys. Rev. B **1**, 2211 (1970).

[14] H. W. de Wijn, L. R. Walker, and R. E. Walstedt, Phys. Rev. B **8**, 285 (1973).

[15] R. J. Christianson, R. L. Leheny, R. J. Birgeneau, and R. W. Erwin, Phys. Rev. B **63**, 140401(R) (2001).

[16] H. K. Lee, D. P. Landau, and T. C. Schulthess, J. Appl. Phys. **93**, 7643 (2003).

[17] D. J. Breed, Physica (Amsterdam) **37**, 35 (1967).

[18] R. A. Cowley, A. Aharony, R. J. Birgeneau, R. A. Pelcovits, G. Shirane, and T. R. Thurston, Z. Phys. B: Condens. Matter **93**, 5 (1993).

[19] N. W. Ashcroft and N. D. Mermin, *Solid State Physics* (Brooks-Cole, Belmont, MA, 1976), Chap. 32, p. 673.

[20] M. E. Lines, Phys. Rev. **164**, 736 (1967).

[21] H. Benson and D. L. Mills, Phys. Rev. **178**, 839 (1969).

[22] R. N. Costa Filho, M. G. Cottam, and G. A. Farias, Phys. Rev. B **62**, 6545 (2000).

[23] U. Wolff, Phys. Rev. Lett. **62**, 361 (1989).

[24] Y. Miyatake, M. Yamamoto, J. J. Kim, M. Toyonaga, and O. Nagai, J. Phys. C **19**, 2539 (1986).

[25] D. Loison, C. Qin, K. D. Schotte, and X. F. Jin, Eur. Phys. J. B **41**, 395 (2004).

[26] C. Zhou, M. P. Kennett, X. Wan, M. Berciu, and R. N. Bhatt, Phys. Rev. B **69**, 144419 (2004).

[27] For a recent example of cutoff applied to dipolar interactions in Monte Carlo simulations of Heisenberg models, see A. P. Rapini, R. A. Dias, and B. V. Costa, Phys. Rev. B **75**, 014425 (2007).

[28] A. M. Ferrenberg and R. H. Swendsen, Phys. Rev. Lett. **61**, 2635 (1988).

[29] D. P. Landau and K. Binder, *A Guide to Monte Carlo Simulations in Statistical Physics* (Cambridge University Press, 2000).

[30] P. G. Maier and F. Schwabl, Phys. Rev. B **70**, 134430 (2004).

[31] J. V. José, L. P. Kadanoff, S. Kirkpatrick, and D. R. Nelson, Phys. Rev. B **16**, 1217 (1977).

[32] E. Rastelli, S. Regina, and A. Tassi, Phys. Rev. B **69**, 174407 (2004).

[33] E. Rastelli, S. Regina, and A. Tassi, Phys. Rev. B **70**, 174447 (2004).

[34] K. Binder and D. P. Landau, Phys. Rev. B **30**, 1477 (1984).

[35] B. V. Costa and A. S. T. Pires, J. Magn. Magn. Mater. **262**, 316 (2003).

[36] G. Schmid, S. Todo, M. Troyer, and A. Dorneich, Phys. Rev. Lett. **88**, 167208 (2002).